R & M No. 3844

R &M No. 3844

PROCUREMENT EXECUTIVE, MINISTRY OF DEFENCE

Aeronautical Research Council
Reports and Memoranda

A LONG STROKE ISENTROPIC FREE PISTON HYPERSONIC WIND TUNNEL

by

R.A. East and A.M.S. Qasrawi
University of Southampton

London: Her Majesty's Stationery Office
£10 NET

A LONG STROKE ISENTROPIC FREE PISTON HYPERSONIC WIND TUNNEL

By R.A. East and A.M.S. Qasrawi

University of Southampton

REPORTS AND MEMORANDA No.3844*

August 1978

SUMMARY

The application of a long stroke isentropic free piston compressor as the energy source for an intermittent M = 6.85 hypersonic wind tunnel is described. The advantages of comparatively long running times of up to 0.5 s and uniform reservoir conditions at up to 90 bar and 600 K are discussed. Particular problems arising from the long stroke compression associated with both viscous flow effects and non-steady wave propagation are discussed and solutions suggested. The theoretical operating principles of long stroke compression tubes are presented and experimental results are given for a pilot facility with compression tube diameter of 0.032 m and length to diameter ratio of 120 and for a full scale facility with corresponding values of 0.11 m and 114.

---

* Replaces AASU Report 334, ARC 37889

LIST OF CONTENTS

1 INTRODUCTION

Short duration high Mach number wind tunnels based on the shock tunnel, gun tunnel and arc-heated tunnel and their derivatives have been widely used over the last two decades in obtaining steady aerodynamic data. Generally, these facilities have provided at significantly lower capital cost, running conditions such as Reynolds number and stagnation enthalpy in excess of those obtainable in continuous running wind tunnels. It is perhaps significant, though, that relatively few investigations of non-steady aerodynamic phenomena, such as measurements of dynamic stability, have been made in such facilities. This is attributed to limitations caused by a combination of lack of running time and flow quality. It is the purpose of this Report to describe a light piston compression facility which has been adapted to produce a high Mach number flow of sufficient duration and quality for dynamic stability studies, yet retains the low capital cost feature of intermittent facilities.

Jones *et al*[1] first suggested the principle on which this device is based and reported on successful pilot experiments which demonstrated its feasibility. Subsequently Schultz *et al*[2] reported a larger scale facility designed to provide a reservoir of hot gas suitable for turbine blade cascade experiments. The basic principle employs a light piston, driven by compressed gas (air or nitrogen), to compress the test gas in a short, large diameter tube. On reaching the desired reservoir conditions a quick acting valve or diaphragm opens the nozzle and the volume rate of flow of the test gas is exactly matched by the volume inflow rate of the driver gas behind the piston. This results in extremely steady flow conditions during the running time apart from certain aberrations discussed in later sections.

Oldfield *et al*[3] have proposed the adaptation of this principle to a high Mach number wind tunnel by utilising the light piston compression principle to heat and compress the test gas in a long, small diameter, tube. Following the gas compression, the tube operates in the Ludwieg tube mode[3] once the nozzle valve or diaphragm is opened and is subject to the same running time limitations, based on tube length, as the conventional Ludwieg tube. The mode of operation is known as the LICH mode.

For high pressure (high Reynolds number) applications, the use of a high length/diameter ratio compression tube is attractive from economic arguments. Also, existing shock/gun tunnels employing high length/diameter ratio tubes could be modified to operate in this mode. The present work describes the application of Jones *et al* principle to tubes of such geometry and extends the running time

capability of Oldfield's LICH tube by employing a driver reservoir/baffle plate system. Operation of a 3.18 cm diameter pilot tube with length/diameter ratio of up to 120 at Southampton University has demonstrated that the principles which apply to shorter, larger diameter tubes are still satisfied, but that greater non-uniformities in compressed gas temperature are observed. The details of the mechanism of the piston/wall boundary layer interaction which lead to the temperature non-uniformity have been studied by flow visualisation in a transparent water analogy tube.

The results of the pilot tube study have led to the design of 0.11 m diameter, 12.4 m long compression tube to act as gas supply source for a 0.21 m diameter M = 6.85 hypersonic wind tunnel nozzle. Experimental results obtained from operation of the full scale facility at pressures up to 90 bar and temperature of 605 K are presented in section 3. Particular attention has been devoted to obtaining the largest possible uniform running times by using compression tube pre-heating to 180^{o}C and a preset initial tube temperature gradient to compensate for cooling effects associated with the piston vortex growth during compression.

2 GENERAL OPERATING PRINCIPLES OF LONG STROKE COMPRESSION TUBES

2.1 Basic operating principles

The operating principle of a generalised light piston isentropic compression facility may be described by reference to Fig 1 in which the principal components are indicated. The additional feature introduced in the present work is a 'wave damper' (D) which comprises a gas reservoir and baffle plate (B) assembly. Its purpose, which will be described in more detail in section 2.4, is to eliminate the reflection of the non-steady expansion wave E which originates when the nozzle (N) is suddenly opened.

The mode of compression of the test gas contained in the compression tube (C) is essentially similar for all variants of the device. A supply of driver gas from a large reservoir, choked at the restrictor (R), compresses the test gas, initially contained in tube (C) at pressure p_0 and temperature T_0, via a light piston in a manner in which the pressure increases linearly with time. Operation with an unchoked restrictor and finite reservoir volume results in a rate of pressure rise which decreases with time. The important feature of the operation is the 'matching' condition at which the nozzle diaphragm or quick acting valve opens. This occurs at the instant when the volume flow rate of driver gas into the tube equals the volume flow rate of compressed gas through the nozzle.

Jones *et al*[1] have presented a simple theory of operation, based on steady flow analyses, which gives an adequate description provided the characteristic time for wave propagation in the tube is much shorter than the characteristic time for the tube filling and compression process. For compression tubes of small length/diameter ratio this condition is easily satisfied and both the compression and nozzle flow periods are well described by 'steady' flow theory. Oldfield *et al*[3] have shown that for large length/diameter ratio tubes, the compression process is very similar to that described in Ref 1 but the subsequent test gas nozzle expansion is similar to that in the Ludwieg tube, necessitating a non-steady analysis. Pressure fluctuations arise in the compressed test gas due to the sudden opening of the nozzle diaphragm or valve and these propagate in the tube in a similar manner to the flow in a Ludwieg tube.

The essential difference between the operational mode for large length/diameter (L/d) ratio tubes proposed in the present work and Oldfield *et al*[3] LICH mode is the addition of the 'wave damper' to extend the running time. For such tubes the strength of the non-steady expansion resulting from nozzle opening is usually greater since there is often a requirement for a fixed ratio of nozzle throat area A_a^* to compression tube volume V_0 to achieve a given running time.

For an effectively closed inlet to the compression tube, wave reflections result in the familiar fall in pressure with time experienced in the Ludwieg tube. The purpose of the wave damper is to eliminate the reflection of the non-steady expansion by matching the steady viscous flow through a baffle plate to the flow behind the non-steady expansion. Experiments on a pilot tube of L/d = 120 have proved the principle of operation and an optimum open/closed area ratio for the baffle plate has been deduced. Further details and a theoretical description of the operation of the wave damper are given in section 2.4.

2.2 Piston oscillation considerations

Jones *et al*[1] equations for predicting the performance variables at matched conditions, together with non-ideal effects due to oscillations of the finite mass piston, may be used for large values of L/d and with the wave damper added provided account is taken of the extra volume introduced. Thus for the modified tube the rate of rise of tube pressure during compression is

$$\left(\frac{dp}{dt}\right)_c = \gamma\beta A_a^* \bar{a}_a \frac{\bar{p}}{W} \qquad (1)$$

where W is the *total* volume of the compression tube and wave damper and $\bar{p}$ is the matching pressure. The volume of the compression tube is denoted by kW where

$$k = \frac{V_0}{W} \quad . \tag{2}$$

The piston velocity at the matching condition at the instant before nozzle opening denoted by suffix d, is given by

$$U_{p_d} = \frac{V_{a_d}}{\gamma A_c \bar{p}} \left(\frac{dp}{dt}\right)_c \quad . \tag{3}$$

After nozzle opening the matching velocity required is determined by the nozzle mass flow rate and is given by

$$\bar{U} = \frac{\beta \bar{a}_a A^* a}{A_c} \quad . \tag{4}$$

A piston of finite mass M is unable to accelerate instantaneously to this velocity and the pressure immediately following nozzle opening initially falls and the piston oscillates about the matching condition. Jones *et al*[1] have presented a linear analysis of the piston oscillation in which pressure and volume changes on both sides of the piston are related isentropically. The period and amplitude of the oscillations are dependent on the relative mass of the piston and the gas contained in the tube. The period of the piston motion is given by[1]

$$\tau = 2\pi \left(\frac{V_a V_b}{\gamma W A_c^2}\right)^{\frac{1}{2}} \left(\frac{M}{\bar{p}}\right)^{\frac{1}{2}} \tag{5}$$

where

$$V_a = \left(\frac{p_0}{\bar{p}}\right)^{1/\gamma} kW \tag{6}$$

and

$$V_b = \left(1 - k\left(\frac{p_0}{\bar{p}}\right)^{1/\gamma}\right) W \quad . \tag{7}$$

Thus equation (5) may be written as

$$\frac{\tau a_0}{2L} = \frac{\pi}{k^{\frac{1}{2}}}\left[\left(\frac{p_0}{\bar{p}}\right)^{1/\gamma}\left(1 - k\left(\frac{p_0}{\bar{p}}\right)^{1/\gamma}\right)\right]^{\frac{1}{2}}\left[\frac{M}{W}\frac{RT_0}{\bar{p}}\right]^{\frac{1}{2}} . \qquad (8)$$

The amplitude of the corresponding pressure fluctuation is given by[1]

$$\frac{\Delta p}{\bar{p}} = \frac{\gamma\tau}{2\pi V_a} A_c(u_p - \bar{u}) . \qquad (9)$$

Substituting for u_p and $\bar{u}$ using equations (3), (4) and (1), for τ using equation (8) and V_a using equation (6), the following equation for the pressure fluctuation is obtained.

$$\frac{\Delta p}{\bar{p}} = \frac{\gamma\beta}{k^{\frac{1}{2}}}\frac{A^*_a}{A_c}\left(\frac{\bar{p}}{p_0}\right)^{\frac{1}{2}}\left(1 - k\left(\frac{p_0}{\bar{p}}\right)^{1/\gamma}\right)^{3/2}\left(\frac{M}{W}\frac{RT_0}{\bar{p}}\right)^{\frac{1}{2}} = f_1\left(\frac{M}{W}\frac{RT_0}{\bar{p}}\right)^{\frac{1}{2}} . \qquad (10)$$

The predictions of equations (8) and (10) are compared with experimental data from several facilities having different values of length/diameter ratio in Figs 2 and 3.

In order to define any departures from theory arising from compression tube operation at high values of L/d, a small scale pilot tube of diameter 3.18 cm and length up to 3.8 m was constructed. The tube was adapted to operate at different L/d ratios and with different wave damper and baffle plate geometries. The principal dimensions of the tube are quoted in Fig 2.

Measurements of pressure fluctuations obtained for many different values of piston mass, matching pressure and pressure ratio, for different tube geometries, are correlated on the basis of equation (10) in Fig 2. Good agreement with the prediction of equation (10) is observed over a variation of about 100 in the piston mass parameter $(MRT_0/W\bar{p})$ and for values of L/d from 13 to 120. Experimental scatter increases for low values of $(MRT_0/W\bar{p})$ which is a result of the difficulty of measuring the very low pressure fluctuations at these conditions.

A correlation of experimental measurements of the period of the piston oscillation in Fig 3 shows less satisfactory agreement with the prediction of theory as given by equation (8).

For values of $(MRT_0/W\bar{p})$ in excess of 1.0 the measurements follow the trend of equation (8) but for lower values of the piston mass parameter an almost constant value of $\tau a_0/2L$ is noted. For these measurements good agreement is observed with the period of acoustic oscillation of gas contained in the whole length of the compression tube. Thus when the piston mass is large compared with the mass of the effective gas spring the period of oscillation is determined from the ratio of the mass to the effective stiffness. For relatively low piston masses the acoustic resonance of the relatively greater mass of the gas column is the important feature.

2.3 Non-steady flow considerations

The departures from the ideal 'matched' flow condition for large length/diameter ratio tubes may be described by reference to Fig 1. It is assumed in this that the piston speed is low enough compared with wave propagation speed for non-steady phenomena during the compression phase to be ignored. On nozzle opening at time t_1 a non-steady expansion wave of strength

$$\frac{\Delta p}{\bar{p}} = \gamma\left(\frac{2}{\gamma+1}\right)^{(\gamma+1)/2(\gamma-1)} \frac{A^*}{A} \qquad (11)$$

is formed, which propagates downstream in the compression tube.

Interaction of this wave with the piston at point A in general results in a transmitted expansion wave E and a reflected expansion wave E' whose relative strengths are determined by the piston mass.

For a zero mass piston the wave will be completely transmitted at the point A with no reflection and the piston will instantaneously increase its speed to that required to meet the zero reflected wave strength condition. For a heavy piston, the inertia prevents sudden acceleration to meet this condition and a piston oscillation results which is dependent on its mass and the relative stiffness of the 'air spring'.

Following its transmission across the piston, the expansion E propagates through a region of non-uniform density which results in a continuous reflection of weak waves which appear as a distributed compression on arrival in the reservoir region. The transmitted expansion E reflects from the baffle plate B either as a compression (shown in Fig 1), or an expansion, dependent on the ratio of the baffle plate open area A_B to the tube area A_C. If the wave damper area A_D is large in comparison with the tube area A_C the wave transmitted

into the damper is of negligible strength. The subsequent principal waves are indicated on Fig 1. Subsidiary wave interactions, together with the reflection of the distributed compression, have been omitted for clarity. In practice, effects due to finite nozzle diaphragm opening time and viscous dissipation, reduce the strengths of all of the waves after several reflections. During these wave reflections the mean flow of gas through the nozzle N results in the piston arriving at the end of the compression tube at time t_4. The mean speed of the piston between times t_1 and t_4 is the matching speed $\bar{U}$. Sudden deceleration from $\bar{U}$ to rest on impact with the nozzle face results in a compression wave propagated rearwards into the compression tube.

In summary, four sources of deviation from the ideal matched pressure $\bar{p}$ may be identified:

(1) piston oscillations;

(2) unsteady nozzle opening expansion reflected between the piston face and the end of the compression tube;

(3) the distributed compression generated by the propagation of the unsteady nozzle opening expansion through the variable density region behind the piston;

(4) the acoustic wave, reflected between the two extremes of the compression tube.

2.4 Operation of the wave damper

By matching the changes of pressure and velocity caused by steady flow through the baffle plate, to those required by the non-steady expansion E, the wave reflected from the baffle plate may be eliminated.

Conditions in the damper reservoir vary during the compression cycle but it is assumed that the reservoir is sufficiently large that negligible changes of pressure are caused by the wave transmitted into it. The steady flow through the baffle plate is described by assuming incompressible orifice flow with a discharge coefficient C_D. Thus the pressure drop is related to the volume flow rate by the following equation:

$$A_C u = \frac{C_D A_B}{\left(1 - \left(\frac{A_B}{A_C}\right)^2\right)^{\frac{1}{2}}} \left(\frac{p_D - p}{\rho}\right)^{\frac{1}{2}} \qquad (12)$$

where p and u are the pressure and velocity at any instant in the compression tube. The Reynolds numbers of the orifice flow are sufficiently high that the

discharge coefficient is independent of Reynolds number and only weakly dependent on the area ratio A_B/A_C . A constant value of C_D equal to 0.61 has been assumed.

Changes of velocity are related to changes of the tube pressure and may be obtained by differentiating equation (12). To first order,

$$du = -\frac{A'}{2u}\,dp \tag{13}$$

where $A' = \dfrac{2C_D^2\alpha^2}{\rho(1-\alpha^2)}$

and $\alpha = \dfrac{A_B}{A_C}$.

For the incident non-steady expansion i changes of velocity and pressure are related by

$$(du)_i = -\frac{a}{\gamma p}\,(dp)_i \tag{14}$$

and for the reflected non-steady wave r by

$$(du)_r = +\frac{a}{\gamma p}\,(dp)_r \quad . \tag{15}$$

Thus on reflection of the non-steady expansion the total increments of pressure and velocity are respectively

$$dp = (dp)_i + (dp)_r$$

$$du = (du)_i + (du)_r \quad .$$

Matching the requirements of the non-steady wave to those for the steady orifice flow using equations (13), (14) and (15) gives

$$-\frac{A'}{2u}\left((dp)_i + (dp)_r\right) = \frac{a}{\gamma p}\left((dp)_r - (dp)_i\right)$$

where the waves are assumed weak. Thus the ratio of the reflected wave pressure to that of the incident wave is given by

$$\frac{(dp)_r}{(dp)_i} = \frac{1 - \varepsilon}{1 + \varepsilon} \tag{16}$$

where $\varepsilon = \frac{C_D^2}{M_c} \frac{\alpha^2}{1 - \alpha^2}$

and M_c is the flow Mach number in the compression tube at the instant of the wave interaction.

For $\varepsilon \to 0$, corresponding to a completely closed baffle plate, the reflected wave strength is of the same sign and equal to the incident wave strength. For $\varepsilon \to \infty$, corresponding to the no-baffle case ($A_B/A_C \to 1.0$), the reflected wave is of opposite sign to the incident wave. The condition for the reflected wave to be eliminated occurs when $\varepsilon \to 1.0$, *ie* when $\alpha = A_B/A_C$ given by

$$\alpha^2 = \left(\frac{1 + C_D^2}{M_C} \right)^{-1} . \tag{17}$$

Comparison of the predictions of equation (16) with measurements of the incident and reflected wave strength from the 3.18 cm diameter pilot facility are shown in Fig 4. Good agreement between theory and experiment is observed for values of the open baffle plate area to tube area between 0.16 and 0.44 and elimination of the reflected wave was observed at $A_B/A_C \simeq 0.18$ compared with the theoretical value for the pilot tube of 0.186.

Experiments with wave dampers of different volumes were also carried out to determine the minimum practical value required for effective operation. Values of k $(= V_0/W)$ less than 0.76 were found to have no further effect on the operation of the wave damper. For values of the damper volume less than about 25% of the total volume some deterioration of performance could be expected due to the non-zero strength of the transmitted non-steady expansion.

2.5 Uniformity of reservoir temperature

Ideally, the reservoir temperature achieved after light piston compression is related to the compression ratio by the isentropic expression

$$\frac{\bar{T}}{T_0} = \left(\frac{\bar{p}}{p_0}\right)^{(\gamma-1)/\gamma} .$$

Measurements of reservoir temperature in compression tubes having L/d ratios of order 10 or less show that the reservoir temperature closely approaches this value for compression ratios up to about 6.0. The main deviation from theory which has been previously reported occurs when the compressed gas is expelled through the nozzle and observations have shown that the final 15-20% of the running time contains gas at a much lower temperature. This has been attributed[1] to the vortex formed ahead of the piston when it accelerates to the matching velocity. This vortex contains the tube boundary layer gas which has been 'scraped' from the wall and has therefore lost heat to the cooler tube during the matched period.

Measurements of reservoir temperature in the Southampton University pilot tube (L = 3.81 m, d = 0.032 m) reported by Turner[4] showed that for values of L/d of order 100 important departures from the isentropic temperature rise also occurred during the compression phase. Since, under certain conditions, a fall in temperature was observed (see Fig 5) before the compression phase had been completed, it is suggested that this phenomenon is the result of a vortex formed during compression. Although the gas within the boundary layer is gaining energy due to compression, heat transfer to the wall causes it to lose energy; resulting in lower energy gas within this layer. This cooler gas is scraped from the tube wall by the piston and forms a reduced energy region which propagates ahead of the piston. Fig 6 shows the estimated position of the piston when the lower energy gas is observed at the nozzle entry for various compression ratios. Also shown for comparison is the calculated piston position at the instant the nozzle opens at the matched condition. It is noted that for values of $\bar{p}/p_0$ in excess of 3.7 the disturbed gas reaches the nozzle entry before the matched condition is attained. Since this phenomenon could affect the uniformity of test conditions in compression tubes of large L/d, a more detailed investigation of the formation of the disturbed region was carried out in a similar transparent water filled tube. This permitted detailed flow visualisation of the formation and growth of this region. Hughes[5], using injected dye, and Khatir[6], using suspended fine charcoal particles, obtained ciné photographic records of the growth of this zone for a range of piston speeds. Fig 7 shows a selection of frames which demonstrate that a vortex is formed ahead of the piston but that this becomes unstable and disturbed fluid from the wall boundary layer propagates in a continuously growing

region ahead of the piston. For higher Reynolds numbers the vortex breakdown occurs more rapidly and the turbulence in the disturbed fluid increases.

A similar investigation reported by Tabaczynski *et al*[7] in a tube of low L/d showed no evidence of the instability observed in Fig 7 since, for their experimental conditions, a discrete toroidal vortex formed in the piston/tube corner and the growth was insufficient for disturbed fluid to reach the centre of the tube. It is suggested, therefore, that the results of Hughes' and Khatir's experiments at high values of L/d are more representative of the phenomenon occurring in high aspect ratio gas compression tubes.

If it is assumed that the low energy fluid contained within the boundary layer of displacement thickness δ^* is scraped by the piston into a region occupying the whole tube diameter ahead then, after the piston has moved a distance dx_p, the corresponding growth of the disturbed zone dX_v, is given by

$$\int_0^{X_v} \frac{\pi d^2}{4}\, dX_v = \int_0^{X_p} \pi d\delta^* dx_p \quad .$$

If the boundary layer growth is given by $\frac{\delta^*}{x_p} = \frac{\text{constant}}{Re_{x_p}^n}$

then

$$X_v d = \frac{C}{Re_{x_p}^n} \int_0^{X_p} x_p \left(\frac{X_p}{x_p}\right)^n dx_p$$

or

$$\frac{X_v d}{X_p^2} = \frac{C}{2-n} \frac{1}{Re_{x_p}^n} \qquad (18)$$

where X_p and X_v are respectively the distance moved by the piston and the distance ahead of the piston occupied by the disturbed fluid, C is a constant of proportionality and the exponent n reflects the state of the boundary layer. For experiments in the water filled tube, Khatir[6] has found a correlation of his results which give

$$\frac{X_v d}{X_p^{1.8}} \propto \frac{1}{Re_{x_p}^{0.4}} \quad .$$

For laminar boundary layer growth in the tube wall an exponent $n = 0.5$ would be expected.

In gas compression tubes observations of the time at which disturbed cooler gas is indicated by a thermocouple at the nozzle entrance, permit estimates to be made of X_v and X_p for various operating conditions by calculating the piston position for a known pressure ratio. Important differences between the compressible gas filled tube and the incompressible water filled model make direct comparison between the two sets of data very difficult. For the water tube the length of the fluid column remains constant during the piston stroke, whereas for the gas filled tube the length of the gas column ahead of the piston decreases, ideally, isentropically with increase of pressure. An attempt has been made to correct for this by defining an effective length X'_v of the turbulence zone in an equivalent uncompressed gas column as

$$X'_v = \left(\frac{p}{p_0}\right)^{1/\gamma} X_v$$

where p is the pressure at the instant when the measurement of X_v is taken.

Difficulty is also encountered with the appropriate definition of the Reynolds number characterising the phenomenon. In general, the Reynolds number during compression, based on piston stroke, is given by

$$(Re)_{x_p} = \frac{\rho u_p}{\mu} X_p \quad .$$

The values of ρ, u_p and μ are given in terms of their initial values at the start of compression by

$$\frac{\rho}{\rho_0} = \left(\frac{p}{p_0}\right)^{1/\gamma}$$

$$\frac{u_p}{u_{p_0}} = \left(\frac{p_0}{p}\right)^{(\gamma+1)/\gamma}$$

and

$$\frac{\mu}{\mu_0} = \left(\frac{p}{p_0}\right)^{3(\gamma-1)/4\gamma} \qquad \text{if } \mu \propto T^{\frac{3}{4}}$$

Hence

$$(Re)_{x_p} = \left(\frac{p_0}{p}\right)^{1.21} (Re_0)_{x_p} \qquad \text{for } \gamma = 1.40$$

where $(Re_0)_{x_p} = \dfrac{\rho_0 u_{p_0} X_p}{\mu_0}$,

which shows how the Reynolds number varies during the compression stroke. For the purpose of correlating the experimental data $(Re_0)_{x_p}$ has been used.

The experimental observations of the growth of the turbulent zone ahead of the piston are shown in Fig 8. Good agreement is observed between the results for the well defined experimental situation in the water tube and the prediction of the simple theory for an assumed laminar tube boundary given by equation (18). However, this theory does not provide a basis for correlating the results from both the pilot and full scale gas compression tubes having L/d of order 100. The growth of the disturbed gas zone is consistently higher than theory for an assumed turbulent wall boundary layer although the agreement improves with increase of Reynolds number. It is suggested that the simple model, which assumes uniform velocity throughout the fluid ahead of the piston, is unsatisfactory in providing a description of the compressed gas zone in which the velocity decreases continuously from the piston velocity near its face to zero at the end wall. Clearly, a more detailed theory which includes the effects of (i) gas compression on the growth of the turbulence zone; (ii) the external velocity gradient on the tube boundary layer; and (iii) the time varying piston velocity is required to accurately model the phenomenon in gas compression tubes. Thus the water tube experiments are unable to provide a quantitative estimate of the growth of the disturbed gas zone but do give an insight into the broad features of the phenomenon occurring during the compression phase.

The principal conclusions for tubes of large L/d which are evident from Fig 8, with regard to departures from isentropic temperatures, are:

(i) for high values of Re_{x_p} the value of $(X_v'd)/X_p^2$ decreases and the zone occupied by the cool gas decreases. Thus as expected the phenomenon is of less importance as the Reynolds number increases for fixed L/d.

(ii) For a given Reynolds number, the value of $(X_v'd)/X_p^2$ is constant and tubes having low values of L/d will have correspondingly low values of X_v'/X_p. The phenomenon is therefore of less importance for short, large diameter compression tubes.

In addition to the temperature drop resulting from the unstable vortex formed during compression, observations in gas compression tubes of large L/d ($\sim$ 100) show that the last 15-20% of the running period contains even cooler gas. This is attributed to the cool gas within the vortex formed at matching and is similar in extent to that reported by Jones *et al*[1] for a compression tube having a value of L/d = 12. This loss of running time is inherent in the operation of such tubes and no attempt has been made to overcome it. However, for a full scale facility based on this concept, the more gradual loss of temperature resulting from the unstable compression vortex has been compensated for by introducing an initial temperature gradient in the gas by preheating the compression tube in a non-uniform manner (see section 3.2.2).

3 FULL SCALE TUNNEL

3.1 Description of tunnel mechanical design and operational capacity

Fig 9 shows a schematic diagram of the full scale tunnel and its main dimensions. The gas supply system is shown schematically in Fig 10. There are three storage vessels of volume 0.65 m^3 each with a maximum working pressure of 165 bar. Two of these vessels are used as a high pressure storage. The driver gas is carried from the high pressure storage to the damping reservoir through two parallel solenoid valves with a maximum total flow rate of 5.2 scm/s. The driver gas flow rate is adjusted by using different reservoir throat sizes upstream of the solenoid valves. The third vessel is used as a low pressure storage in which the driver gas in the tube is discharged after a run. Commercial nitrogen is used as driver and test gas.

The volume of the damping reservoir is about 23% of the compression tube volume and the ratio of the baffle plate open area to compression tube cross sectional area could be varied from 12.4% to 19.1%.

The compression tube is made up of three lengths of stainless steel tubing of 0.108 m (4.25 in) inside diameter and 0.15 m (5.91 in) outside diameter. The

three lengths (12.4 m total length) were joined together and to the expansion nozzle using screwed flanges and easily demountable 'Grayloc' clamps. A provision for a diaphragm at the end of the first length of the tube was incorporated for possible operation of the facility in the shock tube mode. To achieve longer running times, the compression tube was provided with an electric heating system (15 kW total power) capable of heating the tube from room temperature up to 185°C in three hours. The tube is effectively insulated to minimise heat losses.

The tunnel is provided with an axisymmetric contoured nozzle with a design Mach number of 7.0. The nozzle throat is 0.02 m in diameter and the nozzle exit is 0.21 m in diameter. Melinex or metallic diaphragms are used at the nozzle inlet to achieve different matching pressures. Table 1 lists the type and thicknesses of diaphragms used and the corresponding bursting pressures at preheated tube temperature of 175-195°C.

The corresponding free stream Reynolds number varies at a stagnation temperature of 605 K from 6.33×10^6/m to 40.7×10^6/m.

Two aluminium alloy pistons are used; a lighter one (0.29 kg) for pressures up to 60 bar and a heavier one (0.435 kg) for higher pressures.

The tunnel test section is of the open-jet type and is provided with a convergent-straight-divergent diffuser optimised for maximum pressure recovery with an empty test section. The length of the open-jet could be varied from 0.5 to 1.25 nozzle exit diameters. The diffuser channels the test gas into a dump tank 14 m^3 in volume. Because of the relatively large mass (2.29 kg maximum) of test gas used the pressure rise in test section (which is evacuated prior to a run) after the tunnel run is about five times the static pressure in the jet, hence the necessity of having an efficient diffuser for establishing and maintaining a hypersonic flow. With the present configuration of nozzle, open-jet and diffuser, axisymmetric hyperballistic blunt nosed models with base diameter up to 0.05 m could be tested for static force and dynamic stability measurements at angles of attack up to 17°.

3.2 Results of tunnel testing

Experiments were conducted in order to compare the performance of the full scale tunnel with that of the pilot tube and with the estimates of the theoretical analyses in Ref 1 and in section 2. Pressure transducers were used to measure the stagnation pressure in the compression tube and the pitot pressure in the open-jet. Thermocouples with unheated and heated shields were used to measure the temperature in the nozzle throat area and in the open-jet. Fig 11 shows typical records

of the compression tube pressure, temperature of flow in the test section as indicated by a heated-shield thermocouple and pitot pressures at two points in the open-jet.

3.2.1 Measurements of pressure in the compression tube

Measurements of compression tube pressure serve to determine many of the parameters associated with the tunnel performance. These include: rate of pressure rise during compression, pressure fluctuations due to piston oscillations and due to the expansion wave resulting from diaphragm rupture; the reservoir requirement (driver gas mass flow rate into the compression tube) to achieve matching at different stagnation pressures and how it is affected by the tube pre-heating; and finally the running time as determined by the pressure ratio and the initial temperature of the compression tube.

The experimental values of the rate of pressure rise in the compression tube and of the running time for the pilot tube and the large tunnel are compared with the theoretical values from Jones' analysis[1] in Fig 12. From this Figure it may be seen that the experimental values agree well with the theoretical predictions.

Pre-heating of the compression tube was used to increase the running time of the tunnel. Nominal tube temperatures of 100°C and 180°C were employed. Fig 13 shows the experimental values of the running time at these temperatures and for an unheated tube and comparison of these values with the theoretical estimates. It is seen that the experimental values of the running time are smaller than the theoretical predictions. This is caused by the heat losses to the wall of the tube which necessitates the operation at a higher compression ratio than that predicted by isentropic compression theory to achieve a specific value of the stagnation temperature. The departure of the experimental value from the theoretical one becomes relatively smaller at higher initial temperatures of the compression tube because of the lower rates of heat transfer to the wall from the test gas.

One interesting result of testing the large scale tunnel was that the reservoir mass flow rate required to achieve matching at a certain stagnation pressure was affected by the initial temperature of the compression tube. The reason for this effect is believed to be the heat transfer from the hot walls of the compression tube to the driving gas throughout the compression and the matched periods of the run. The increase in temperature of the driving gas due to this heat transfer causes a rise in pressure behind the piston above the expected

values for the particular mass flow rate. This pressure rise is partly offset by a pressure drop in the region ahead of the piston caused by a similar but opposite heat flow from the test gas, heated by compression, to the colder walls of the compression tube. A heat transfer analysis was carried out to estimate these effects on the matching process assuming turbulent flow on both sides of the piston and using Reynolds analogy and the friction law of Blasius. The results of this analysis show good agreement with the experimental observations. The heat transfer analysis is outlined in brief in the Appendix.

3.2.2 Measurements of temperature in the nozzle throat area and in the open-jet

Measurements of the temperature in the nozzle throat region were made using a thermocouple, with an unheated shield, which has recovery factors very close to unity at Mach numbers of up to 1.0. The peak temperatures recorded are shown in Fig 14 for different pressure ratios with the compression tube at ambient temperature. It is seen that the measured temperatures approach the values estimated from isentropic compression theory at low pressure ratios when the temperature records show a plateau at the beginning of the running time followed by a steady fall in the temperature caused by the cooling effect of the compression vortex and a steeper fall during the last 15% of the running time caused by the second vortex generated ahead of the piston at the moment of the flow start. This temperature plateau decreases in duration with the increase in the pressure ratio till it disappears altogether and the recorded peak temperatures fall much below the estimates from the isentropic compression theory. As was expected (see section 2.5), the effect of the compression vortex on the flow temperature was less severe than in the pilot tube as the surface area/volume ratio is smaller for the full scale tunnel. This effect was eliminated by pre-heating the tube with a suitable temperature gradient to compensate for the loss of enthalpy. A thermocouple with a heated shield[10] utilizing a null operating method shown in Fig 15 was used to measure the stagnation temperature of the flow in the test section. These measurements showed that temperature gradients from 95°C at the nozzle to 120°C at the baffle plate (using a compression ratio of 7.0) and from 175°C at the nozzle to 195°C at the baffle plate (using a compression ratio of 3.26) result in a flow stagnation temperature of 605 K uniform to ±2% during periods of 250 ms and 460 ms respectively. The 15-20% loss of 'hot' running time caused by the second vortex is inherent in this type of compression process and is accepted as unavoidable.

3.3 Test section calibration

Test section calibration involved the measurement of pitot pressure and flow temperature in the open-jet and blockage tests to determine the size of typical hyperballistic shapes that could be tested in the test section at small and moderate angles of attack.

Surveys of pitot pressure in the open-jet indicated that the Mach number was 6.85 ±0.15 in the inviscid core of the jet at stations ranging from the nozzle exit plane to 0.9 exit nozzle diameter downstream. These surveys and measurements of the stagnation temperature in the open-jet demonstrated the effects of changing the length of the jet on the quality of the flow during the running time; reducing the open-jet length from about 3.0 D_N (nozzle exit diameter) to about 1.25 D_N resulted in an appreciable improvement in the steadiness of pitot pressures and stagnation temperature in the test section. For the lower value of open-jet length, the pitot pressure and the stagnation temperature in the inviscid core were uniform to ±2% throughout the running time except for the sudden fall in temperature during the last 15% of the running time.

Blockage tests using typical hyperballistic shapes (blunt cones and hemisphere cylinder-flow type bodies) also highlighted the importance of using a short open-jet to maintain a hypersonic flow with relatively large blockage area as represented by such blunt shapes and typical model sting supports for dynamic stability measurements. Schlieren photography and measurements of the static pressure in the test section plenum were used to establish and assess blockage effects. It was found that the reduction in the open-jet length was beneficial from the blockage point of view, with a short open-jet of 0.5 D_N, hemisphere-cylinder-flare type shapes of base diameters up to 0.05 m could be tested for static force and dynamic-stability measurements at angles of attack up to 17^o. With increase of the angle of attack, the static pressure in the test section plenum rises above the value of the static pressure in the jet up to a maximum pressure ratio of about 2.5 close to the tunnel blockage boundary. Beyond this value of pressure ratio the strong compression waves emanating from the nozzle exit could no longer support the pressure difference and this led to the breakdown of the flow before the end of the run.

The Southampton University light piston tunnel has been used extensively for investigations into the hypersonic dynamic stability of axisymmetric ballistic shapes (10 deg blunt and sharp cones, AGARD standard models HB1 and HB2 and hemisphere cylinder-double flared type bodies). Measurements of the pitching derivatives were successfully carried out at different values of the free stream

Reynolds number, position of the axis of model oscillation (for positive and negative values of the stiffness derivative) and angle of attack using a free-oscillation technique with sting-supported models mounted on crossed flexures for pivots. Typical experimental results of the pitching derivatives for a double-flared model HBS[11] are shown in Fig 16 together with estimates from the Newtonian and embedded Newtonian[12] theories for comparison.

4 CONCLUSIONS

This study has extended the previously reported range of operating conditions for light free piston compression facilities to those appropriate ($\bar{T}_0$ = 605 K, $\bar{p}_0$ = 90 bar) for providing a uniform supply of test gas (nitrogen) to a high Mach number (M = 6.85) wind tunnel nozzle. A relatively long stroke and small diameter tube, which is structurally more efficient for high pressure and high temperature operation, was chosen for this purpose. Greater non-uniformity in the compressed gas temperature was observed for long stroke operation compared with previous results from shorter, larger diameter tubes which are more optimum from reduced surface heat transfer losses considerations. Detailed investigations of the compression process in a long stroke pilot tube and a water filled flow visualisation tube have confirmed that the differences result from a cool turbulent gas zone ahead of the piston caused by scraping of the wall boundary layer by the piston during the compression phase. Uniform compressed gas conditions may be simply achieved in the long stroke tube by compensating for the cool gas region by using a preset initial temperature gradient along the compression tube.

Operation of the full scale long stroke tube at elevated initial temperatures up to 185°C has resulted in relative increases of tunnel running time greater than predicted by simple theoretical analysis. The reduction in heat loss from the test gas to the heated tube provides an explanation. The maximum running time achieved has been 0.54 s at $\bar{p}$ = 90 bar and $\bar{T}$ = 605 K. The excellent flow uniformity during this period has enabled the tunnel to be used for dynamic stability tests on blunt axisymmetric shapes at Reynolds numbers based on body length of up to 6.5×10^6.

Whilst it has been demonstrated that straightforward long stroke operation of free piston compressors does not provide compressed gas conditions which are as uniform as those for short stroke tubes, complete compensation may be obtained using prescribed initial temperature distributions of pre-heated tubes. By using this compensation the following potential advantages of long stroke operation may be fully realised:

(1) the structural efficiency of smaller diameter tubes for the highest pressure applications may be exploited;

(2) existing shock tubes/gun tunnels/Ludwieg tubes of high L/d could be converted to free piston operation.

Thus long stroke operation at high initial pressure could be of value in the proposed application of the free piston principle to an intermittent cryogenic facility proposed by Stollery and Murthy[8]. Long stroke operation, together with pre-heating to about 300°C, also permits the attainment of compressed gas conditions which make the facility attractive for simulating aircraft turbo jet post compressor conditions for combustion studies. A feasibility study[9] of the use of the compression tube described in section 3 as an intermittent hot gas generator for turbo-jet combustor studies has shown that operation at $\bar{p}$ = 50 bar, $\bar{T}$ = 800 K, mass flow ~ 6 kg/s in a 5 cm diameter pipe at M = 0.15 should be possible with a flow duration of 0.25 s.

Acknowledgments

The interest and skill of the technical staff of the Aeronautics and Astronautics Department, University of Southampton, especially Mr G. Wilding and Mr D. Hill, are gratefully acknowledged. The authors also wish to express their gratitude to the Central Design Service, University of Southampton for their assistance with mechanical design problems.

Many helpful discussions with Dr D.L. Schultz, Dr T.V. Jones and Dr M.L.G. Oldfield of the Department of Engineering Science at Oxford University are also gratefully acknowledged.

Appendix

THE EFFECT OF HEAT TRANSFER ON THE MATCHING CONDITION

This analysis was carried out to derive expressions for the rate of change of gas temperature and therefore pressure due to the transfer of heat from the hot wall of the tube to the driver gas and from the hot compressed test gas to the relatively cooler tube wall. An example case is treated and the estimates are compared to the experimental observations.

The shear stress at the wall τ_w is expressed as

$$\tau_w = f \frac{\rho U^2}{2} .$$

f is evaluated experimentally by the friction law of Blasius as

$$f = \frac{0.0791}{Re_d^{1/4}}$$

$$\therefore \tau_w = \frac{0.03955 \rho U^2}{Re_d^{1/4}} . \qquad \text{(A-1)}$$

The rate of heat transfer from the wall to the driver gas (or from the test gas to the wall) for an elemental tube length Udt ($t \equiv$ time) is:

$$q_w = \pm \tau_w Cp \left(\frac{T_{wall} - T_{gas}}{U} \right) \pi d U dt . \qquad \text{(A-2)}$$

From energy balance:

$$q_w = \rho Cp U \frac{\pi d^2}{4} dT . \qquad \text{(A-3)}$$

From (A-2) and (A-3), substituting for ρ and Re_d (using T_{amb} as a reference temperature and assuming $\mu \propto T^{0.76}$) and non-dimensionalising the temperature T_{gas} with respect to T_{wall} ($T' = T/T_{wall}$), the equation governing the temperature-time relation becomes

$$\frac{dT'}{dt} = C_h (1 - T') T'^{0.44} U^{0.75} p^{-0.25} \qquad \text{(A-4)}$$

where $$C_h = \frac{0.1482 T_{wall}^{0.44} (R\mu_{amb})^{0.25}}{d^{1.25} T_{amb}^{0.19}} .$$

For the driver gas during the compression phase[1]:

$$U = \frac{A^* \bar{a}_a}{PA} \quad \text{and} \quad P = p_0 + \left(\frac{\bar{dp}}{dt}\right)_c t$$

where $$\left(\frac{\bar{dp}}{dt}\right)_c = \frac{\gamma \beta A^* \bar{a}_a \bar{p}}{W} = c' ,$$

Substituting in equation (A-4)

$$\frac{dT'}{(1 - T')T'^{0.44}} = C_1 \frac{dt}{P_0 + C't} \tag{A-5}$$

where $$C_1 = C_h \left(\frac{\beta A^* \bar{p}_a \bar{a}_a}{A}\right)^{0.75} .$$

For the driver gas during the running time after the diaphragm bursts[1]

$$U = \bar{U}_p = \frac{\beta \bar{a}_a A^*}{A} ,$$

$$P = \frac{\bar{P} T'}{T'_d}$$

where T'_d is the value of T', as obtained from equation (A-5) at the moment of diaphragm burst. Substituting in equation (A-4)

$$\frac{dT'}{dt} = C_2 (1 - T') T'^{0.19} \left(\frac{T'_d}{\bar{P}}\right)^{0.25} \tag{A-6}$$

where $$C_2 = \left(\frac{C_1}{\bar{P}}\right)^{0.75} .$$

Equations (A-5) and (A-6) could be solved numerically to evaluate T' and dT'/dt at any instant during the running time.

For the test gas equation (A-4) will take the form

$$\frac{d\Delta T'}{(T' - 1)T'^{0.44}} = C_h U^{0.75} p^{-0.25} dt$$

where $\Delta T'$ is the drop in the temperature of the test gas (due to heat losses) below the isentropic compression temperature T_i', *ie*

$$\Delta T' = T_i' - T'$$

$$T_i' = \left(\frac{P}{P_0}\right)^{(\gamma-1)/\gamma}$$

and

$$\frac{P}{P_0} = 1 + \frac{C'}{P_0} t \quad .$$

The equation which governs the temperature-time relation is:

$$\frac{d\Delta T'}{(T_i' - 1 - T')(T_i' - \Delta T')^{0.44}} = C_h U^{0.75} p^{-0.25} dt \quad . \qquad \text{(A-7)}$$

The test gas speed during the compression phase varies from zero at the nozzle end to the value of the piston speed just ahead of the latter. Hence, a mean test gas velocity of half the piston speed is assumed for the compression phase.

Substituting $\frac{1}{2}U_p$ for U in equation (A-7) and solving numerically, the value of $\Delta T'$ at the moment of flow start could be obtained.

During the running time, the test gas is travelling ahead of the piston at the speed of the latter. Transfer of heat to the tube wall is also governed by equation (A-6) with an appropriate negative sign.

The effective rate of increase of flow temperature during the running time is expressed as

$$\left(\frac{dT'}{dt}\right)_{driver} - \left(\frac{dT'}{dt}\right)_{test} \quad .$$

This defines the effective rate of tube pressure rise during the running time due to heat transfer from and to the tube wall.

For the Southampton University large scale tunnel, the following operating conditions were considered:

$$\bar{p} = 6.2 \times 10^6 \text{ N/m}^2 , \quad \bar{T} = 605 \text{ K}, \quad T_{amb} = 288 \text{ K} \quad \text{and} \quad \gamma = 1.4 .$$

Since pre-set temperature gradients were applied along the compression tube to compensate for heat losses from the test gas to the tube wall and the resulting stagnation temperature in the test section was practically constant during the running time, it is reasonable to assume that the heat transfer from the tube wall to the test gas only accounts for any flow undermatching at elevated tube temperatures.

Assuming matched conditions at $T_{wall} = 110^{o}C$, then from the above analysis we find that at the moment of diaphragm rupture

$$\left(\frac{dT}{dt}\right)_{driver} = 36.3^{o}C/S \text{ for } T_{wall} = 180^{o}C \text{ and } 12.8^{o}C/S \text{ for } T_{wall} = 110^{o}C .$$

The effective rate of pressure rise at the moment of diaphragm rupture with $T_{wall} = 180^{o}C$ is calculated to be 4.3 bar/s. This compares well with the experimentally observed rate of pressure rise of about 5.0 bar/s. The corresponding rates, averaged along the running time are 4.0 bar/s, (as calculated analytically) and 4.5 bar/s (as observed experimentally). The agreement is apparently good and suggests that the heat transfer phenomenon proposed is a possible explanation of the observed change in matching conditions at elevated compression tube temperature.

Table 1

TYPE AND THICKNESS OF DIAPHRAGMS USED FOR DIFFERENT PRESSURES

Diaphragms	Total thickness mm	Average bursting pressure in bar
1 Melinex SWG500	0.125	14
1 Melinex SWG1000	0.250	23
1 Melinex SWG500 + 1 Melinex SWG1000	0.375	35
2 Melinex SWG1000	0.50	44
1 Aluminium SWG26	0.45	60
1 Aluminium SWG26 + 1 Stainless steel SWG1000	0.475	78
1 Aluminium SWG25 + 1 Stainless steel SWG150	0.4875	90

LIST OF SYMBOLS

a	speed of sound
A_B	baffle plate open area
A_C	compression tube cross-sectional area
A_D	wave damper cross-sectional area
A^*_a	nozzle throat area
C	constant of proportionality defined in section 2.5
C_D	discharge coefficient for an orifice flow
C_h, C_1, C_2	constants of proportionality defined in the Appendix
Cm_α	pitching moment static derivative, $\dfrac{M_\alpha}{\frac{1}{2}\rho_\infty U_\infty^2 \frac{\pi d^3}{4}}$
Cp	specific heat at constant pressure
$Cm_q + Cm_{\dot{\alpha}}$	pitching moment dynamic derivative, $\dfrac{M_{\dot{\alpha}}}{\frac{1}{2}\rho_\infty U_\infty^2 \frac{\pi d^4}{4}} \dfrac{2U_\infty}{d}$
D_N	nozzle exit diameter
d	compression tube diameter, model centre-body diameter (Fig 16)
k	V_0/W
L	compression tube length
M	piston mass, Mach number or pitching moment
n	boundary layer velocity profile index, $\dfrac{\delta^*}{x_p} = \dfrac{C}{Re_{x_p}^n}$
P	pressure
ΔP	pressure difference or change, amplitude of pressure oscillation
$\left(\frac{dP}{dt}\right)_c$	rate of rise of pressure during compression
q_w	heat transfer rate to or from the compression tube wall
R	gas constant per unit mass
Re	Reynolds number
t	time
T	temperature
T'	temperature non-dimensionalised with respect to tube wall temperature T_{wall}
T'_i	non-dimensionalised temperature from isentropic theory of compression
U	speed
V	volume
V_0	compression tube volume, kW
W	total tube volume, compression tube + wave damper

LIST OF SYMBOLS (concluded)

x_p	distance travelled by piston
x_v	growth of the turbulent zone ahead of the piston
Xc.g.	position of the centre of gravity of an oscillating model from the nose
X_p	piston stroke at the end of compression
X_v	total length of the turbulence zone at the end of compression
X'_v	effective length of the turbulence zone in an equivalent incompressible gas column, $X_v \left(\frac{P}{P_0}\right)^{1/\gamma}$
α	A_B/A_C
β	$\left(\frac{2}{\gamma + 1}\right)^{(\gamma+1)/2(\gamma-1)} = 0.578$ for $\gamma = 1.4$
γ	ratio of specific heats
ε	$C_D^2 \frac{\alpha^2}{1 - \alpha^2}$
ρ	density
τ	period of piston oscillation
τ_{run}	running time
τ_{tube}	tube time = $V_0/\beta a_0 A^*_a$
τ_w	shear stress at the tube wall
μ	viscosity

Suffices

0	initial condition
a	value in region ahead of the piston
b	value in region behind the piston
B	baffle plate
c	compression tube
d	value at the time the nozzle diaphragm bursts or valve opens
D	wave damper
i	incident non-steady wave
p	piston
r	reflected wave
w	tube wall
$\bar{p}$	matching value of P
∞	free stream condition

REFERENCES

No.	Author	Title, etc
1	T.V. Jones D.L. Schultz A.D. Hendley	On the flow in an isentropic light piston tunnel. ARC R & M No.3731 (1973)
2	D.L. Schultz T.V. Jones M.L.G. Oldfield L.C. Daniels	A new transient cascade facility for the measurement of heat transfer rates.
3	M.L.G. Oldfield T.V. Jones D.L. Schultz	A Ludwieg tube with light piston isentropic compression heating. ARC 34 255 (1973)
4	I.D. Turner	A study of the temperature characteristics in the light piston compression tube at Southampton University. University of Southampton BSc Honours Project, March 1975
5	N.A.P. Hughes	Flow visualisation of the complex vortex formed by a piston in a long cylinder. University of Southampton BSc Honours Project, May 1976
6	F.A. Khatir	An investigation into the turbulent fluid zone produced by a moving piston inside a cylinder. University of Southampton BSc Honours Project, May 1977
7	R.C. Tabaczynski D.P. Hoult J.C. Keck	High Reynolds number flow in a moving corner. *J. Fluid Mech.*, 42, p 249 (1970)
8	J.L. Stollery A.V. Murthy	An intermittent high Reynolds number wind tunnel. Unpublished communication (1977)
9	R.A. East	Unpublished work (1978)
10	R.A. East J.H. Perry	A short time response stagnation temperature probe. AASU Report 264 (1966)
11	A.M.S. Qasrawi	Measurements of hypersonic dynamic stability of pitching blunt-nosed bodies in a short-duration facility. University of Southampton PhD Thesis, October 1977
12	L.E. Ericsson	Unsteady embedded Newtonian flow. *Astronautica Acta*, Vol 18, No.5 (1973)

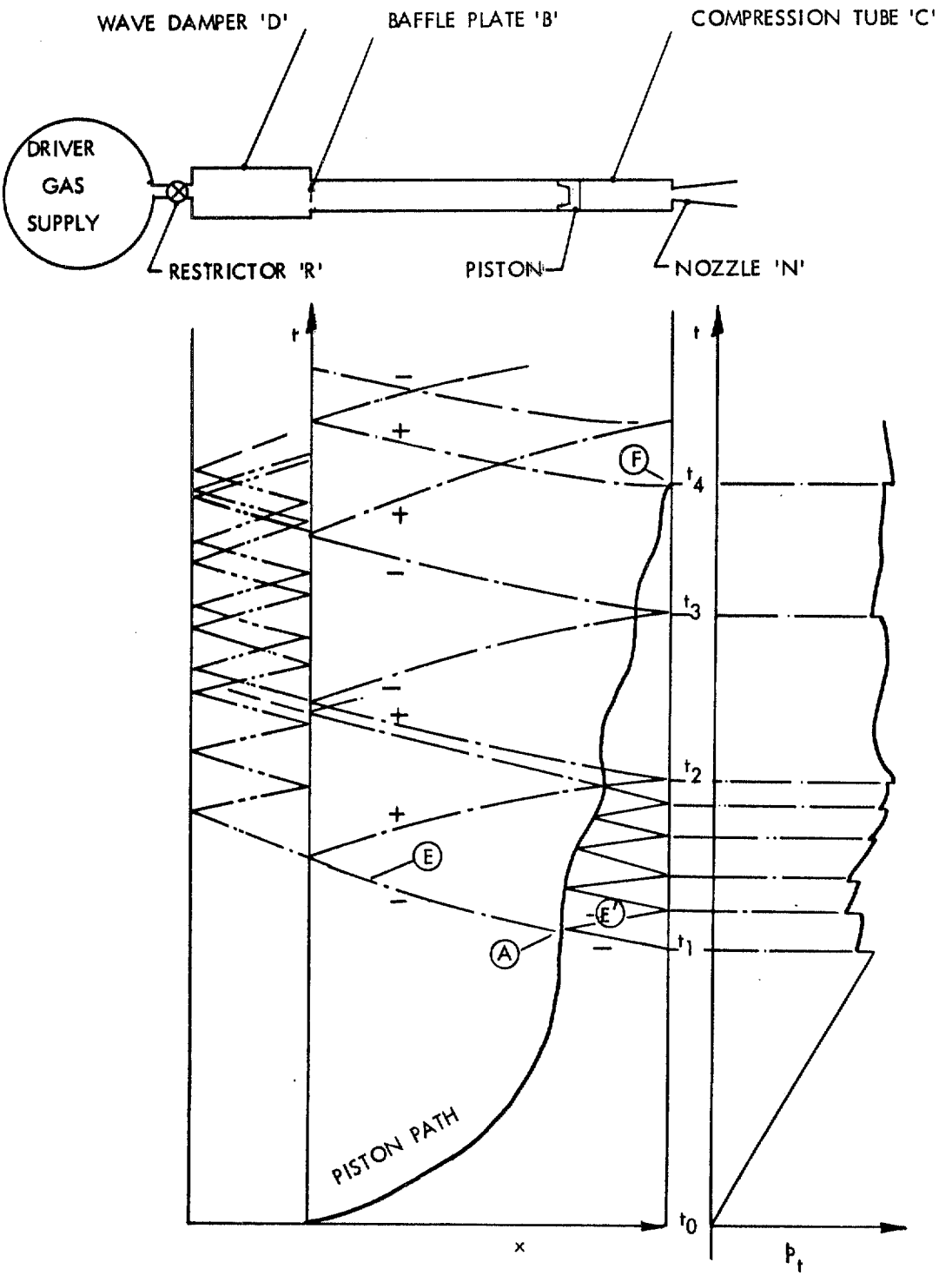

Fig 1 Diagrammatic sketch of a generalised free piston compressor with $x - t$ and $p_t - t$ diagrams

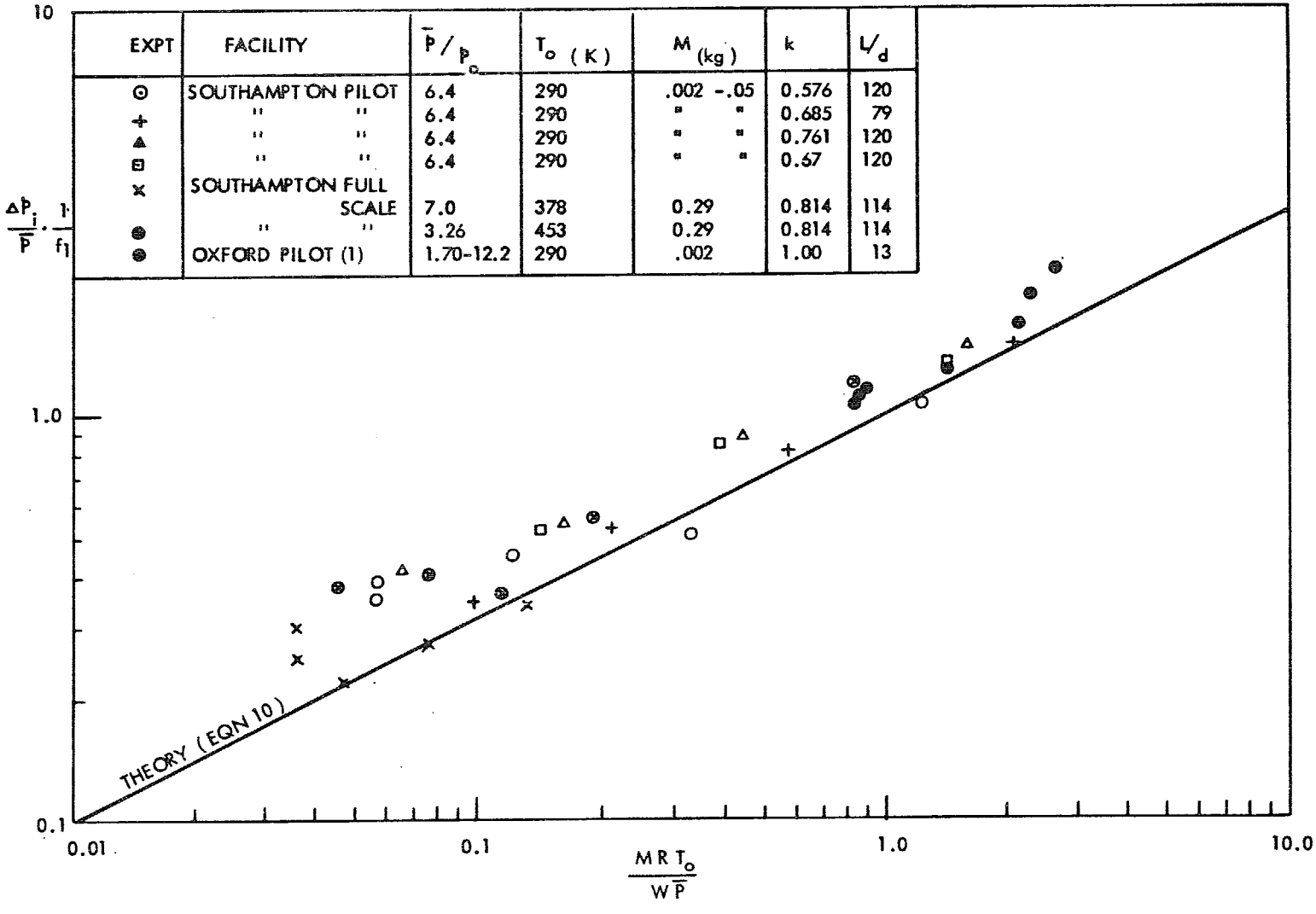

Fig 2 Pressure fluctuations due to piston oscillation: comparison of theory and experiment

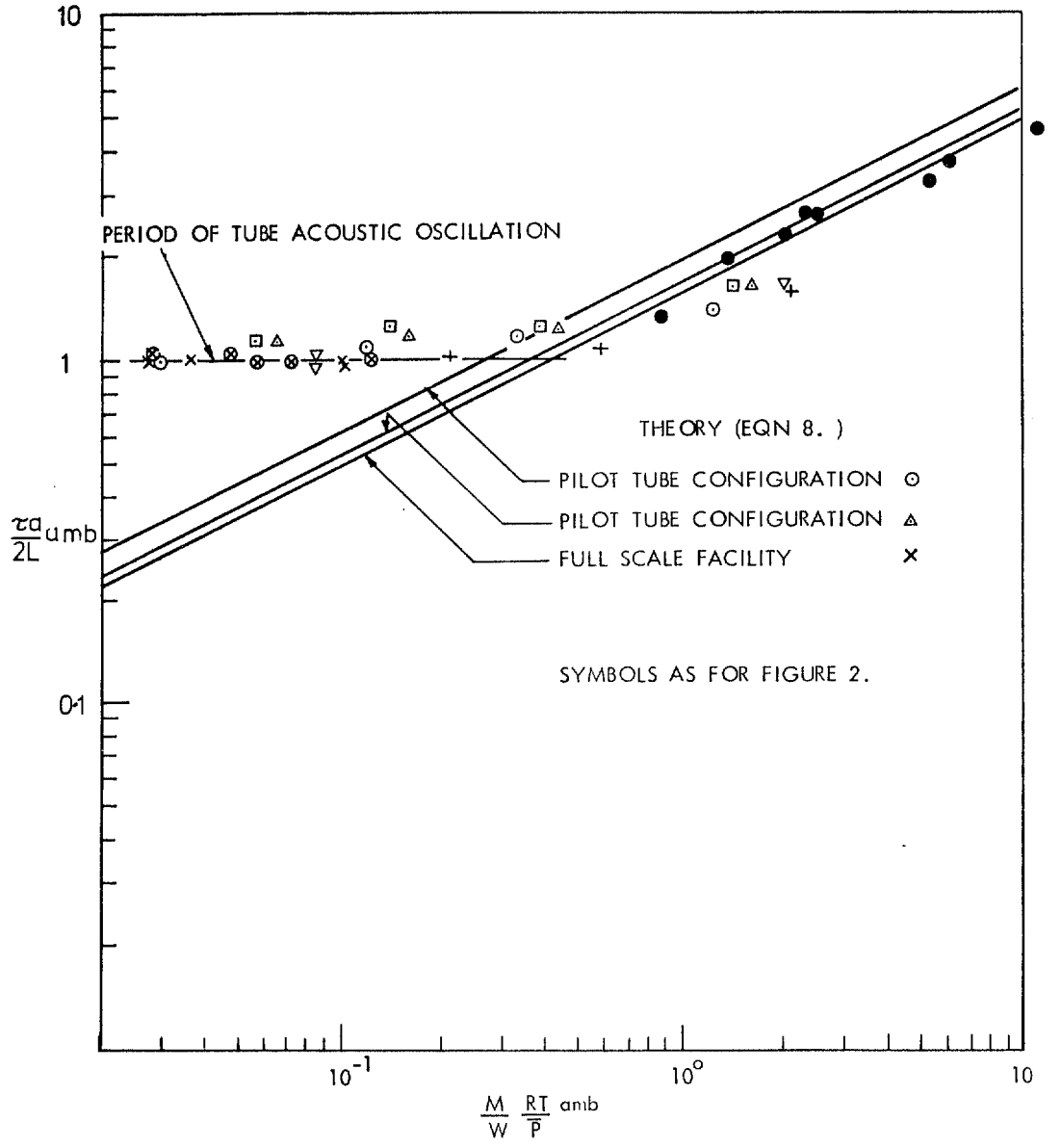

Fig 3 Period of piston oscillation: comparison of theory and experiment

Fig 4

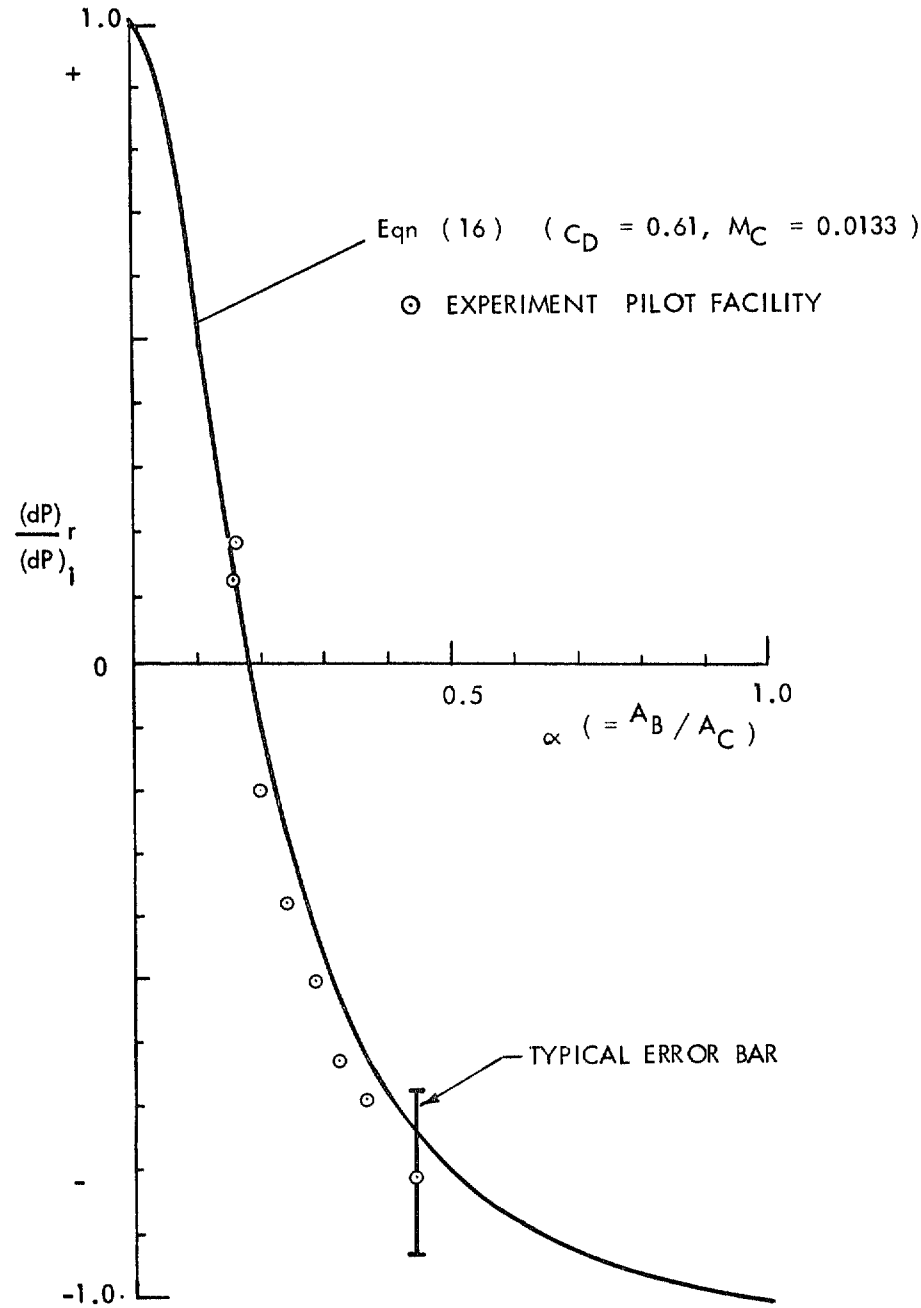

Fig 4 Ratio of reflected/incident wave strength for pilot tube ($M_C = 0.0133$), $\frac{\bar{p}}{p_0} = 6.46$, $d_* = 0.5$ cm, $d_c = 3.17$ cm

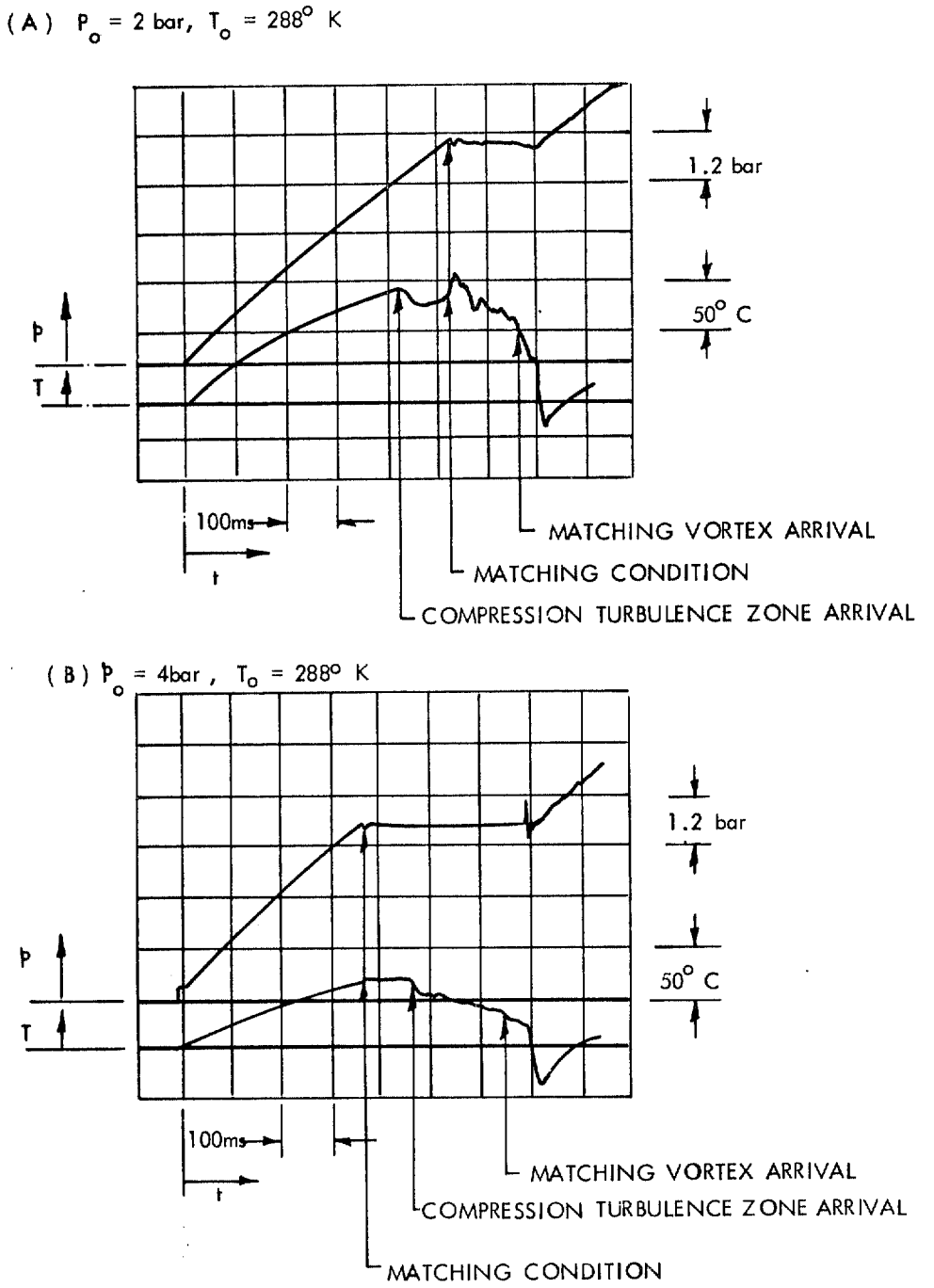

Fig 5a&b Pilot facility p – t and T – t oscillograms
a Turbulence zone arrival before matching
b Turbulence zone arrival after matching

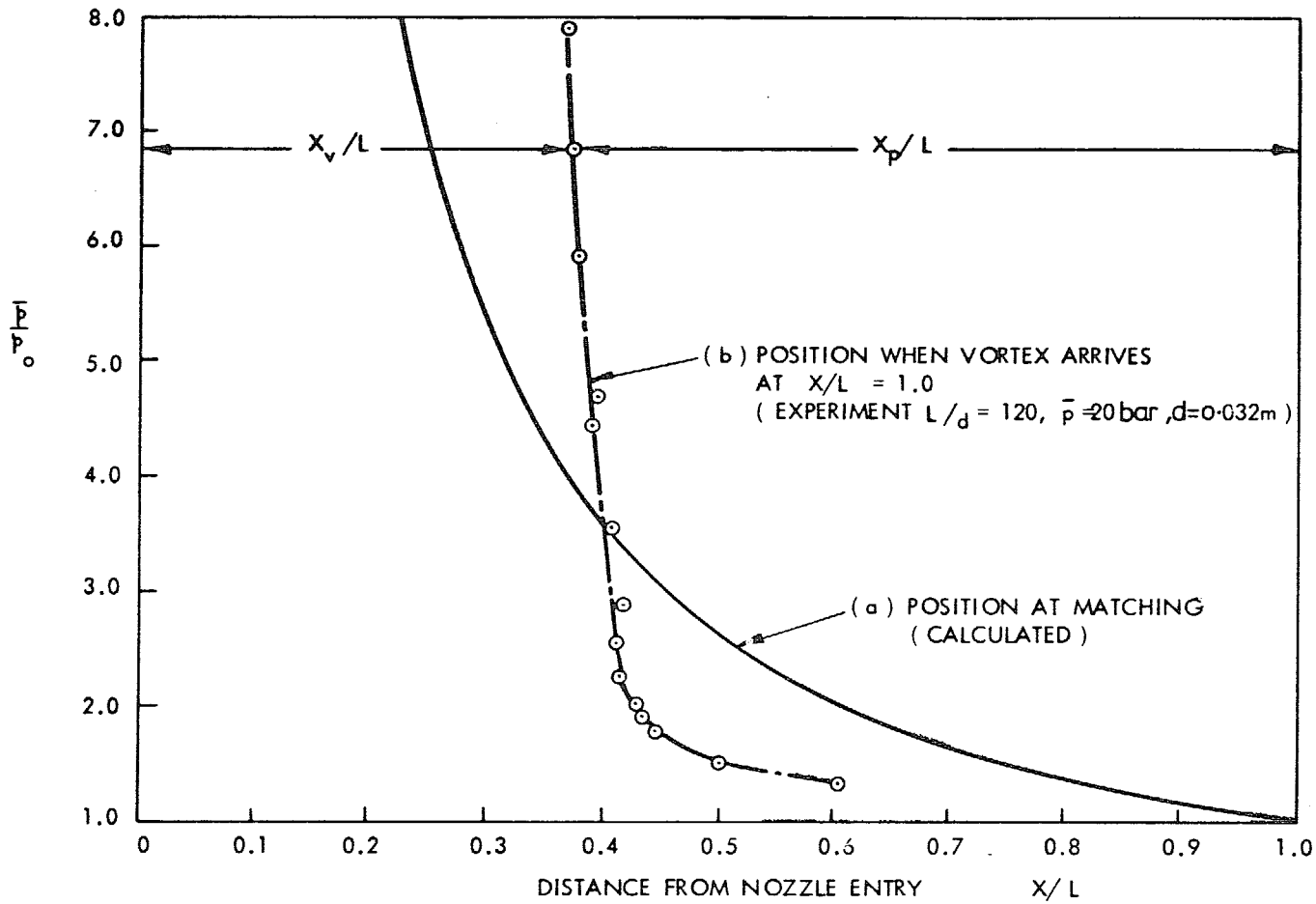

Fig 6 Piston position for various matching pressure ratios (pilot facility)
(a) When matching condition reached
(b) When unstable vortex arrives at end face

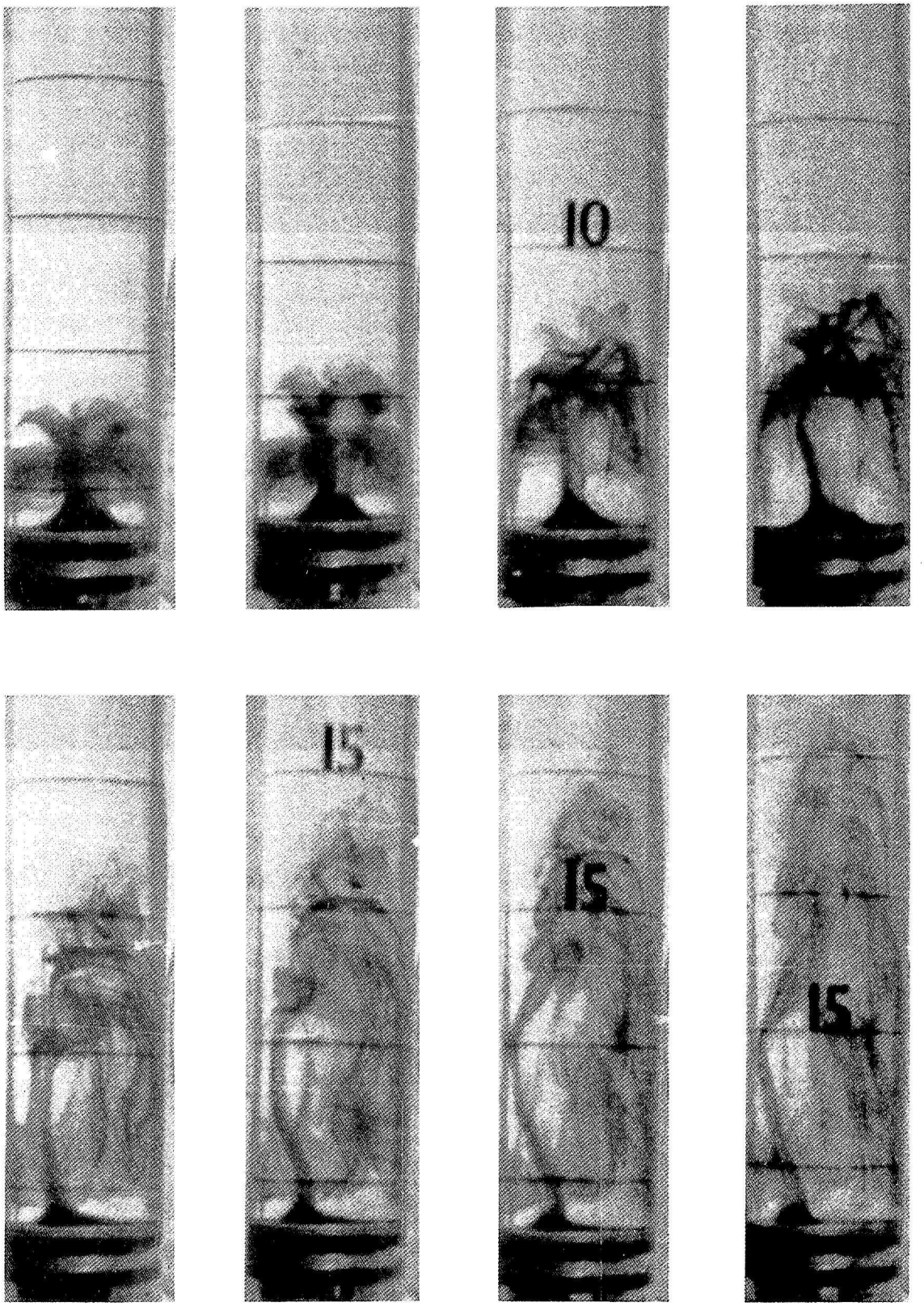

Fig 7 Sequence of photographs showing the formation, growth and break-up of the toroidal vortex ahead of a piston in water $(Re)_d \simeq 2000$

Fig 8

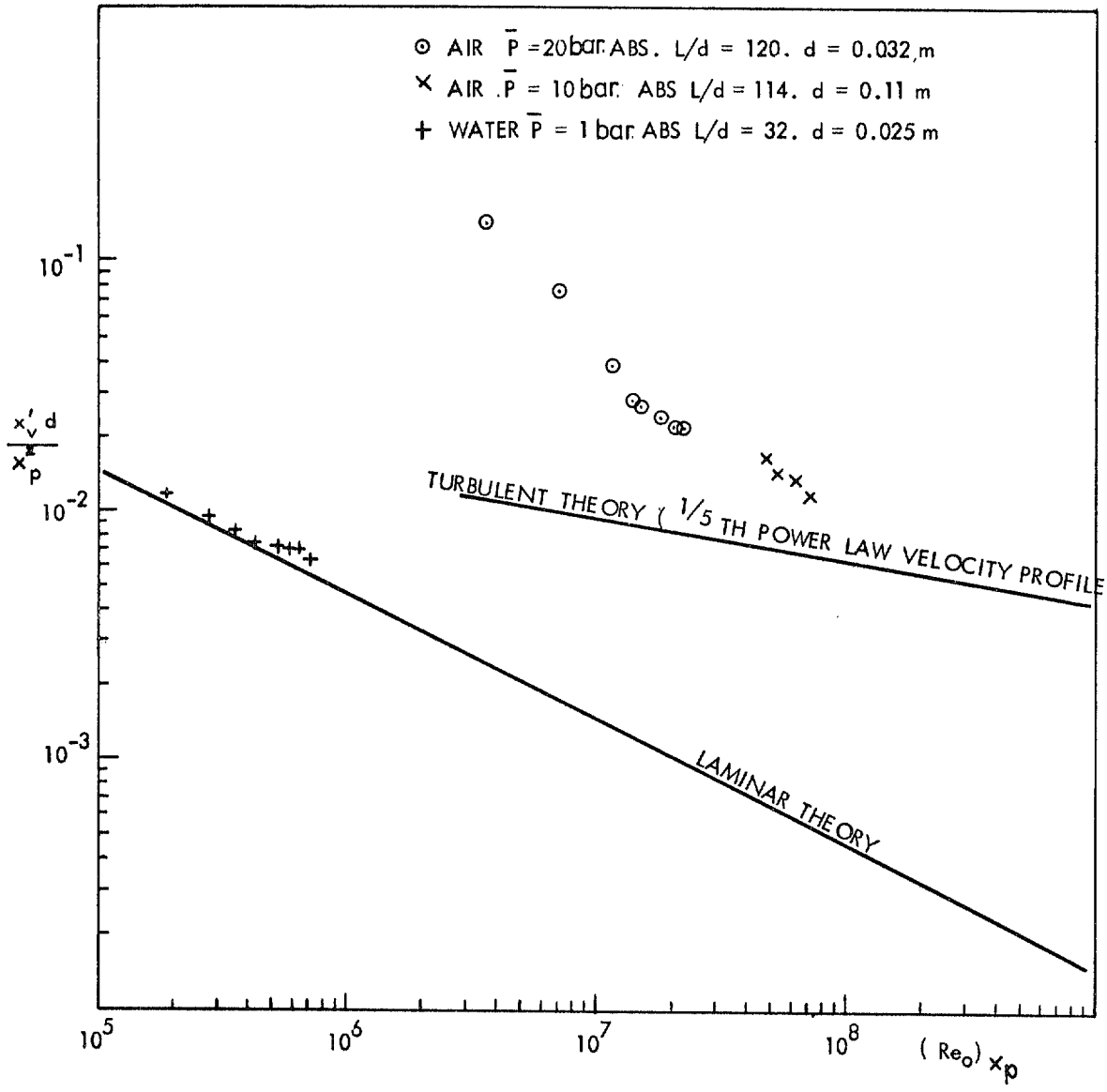

Fig 8 Growth of turbulence zone with Reynolds number based on piston stroke, X_p

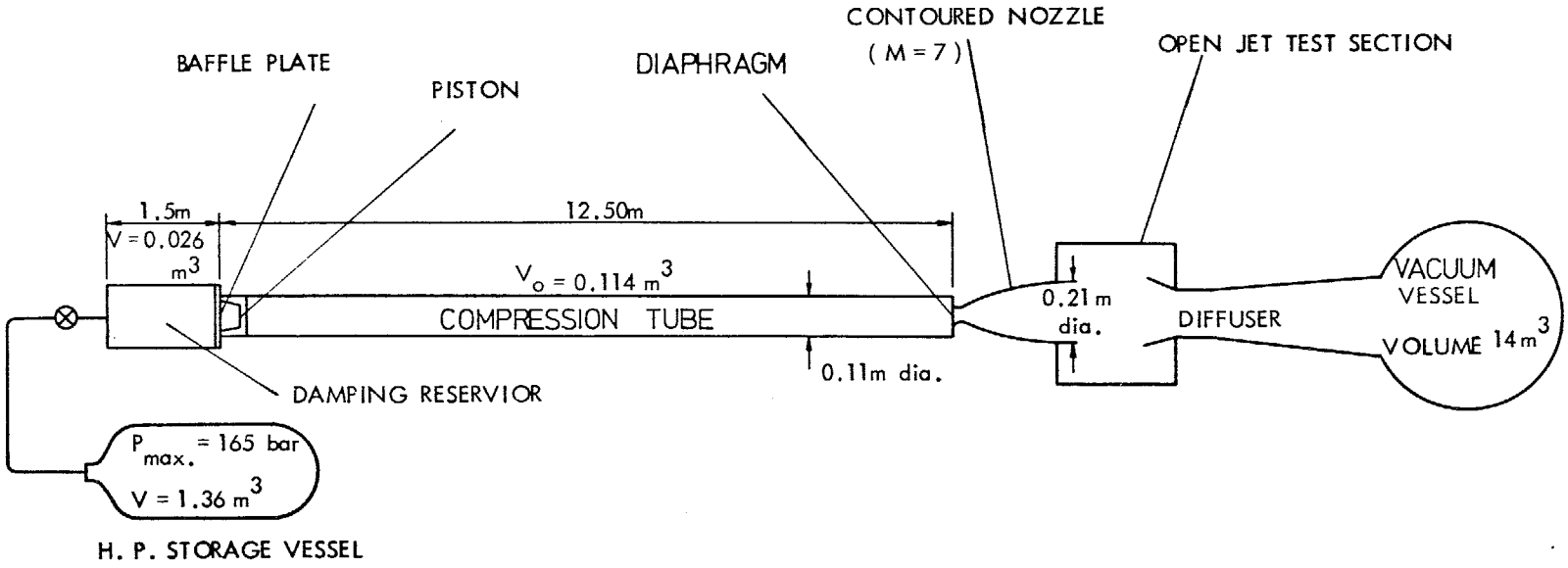

Fig 9 Schematic diagram of large scale tunnel

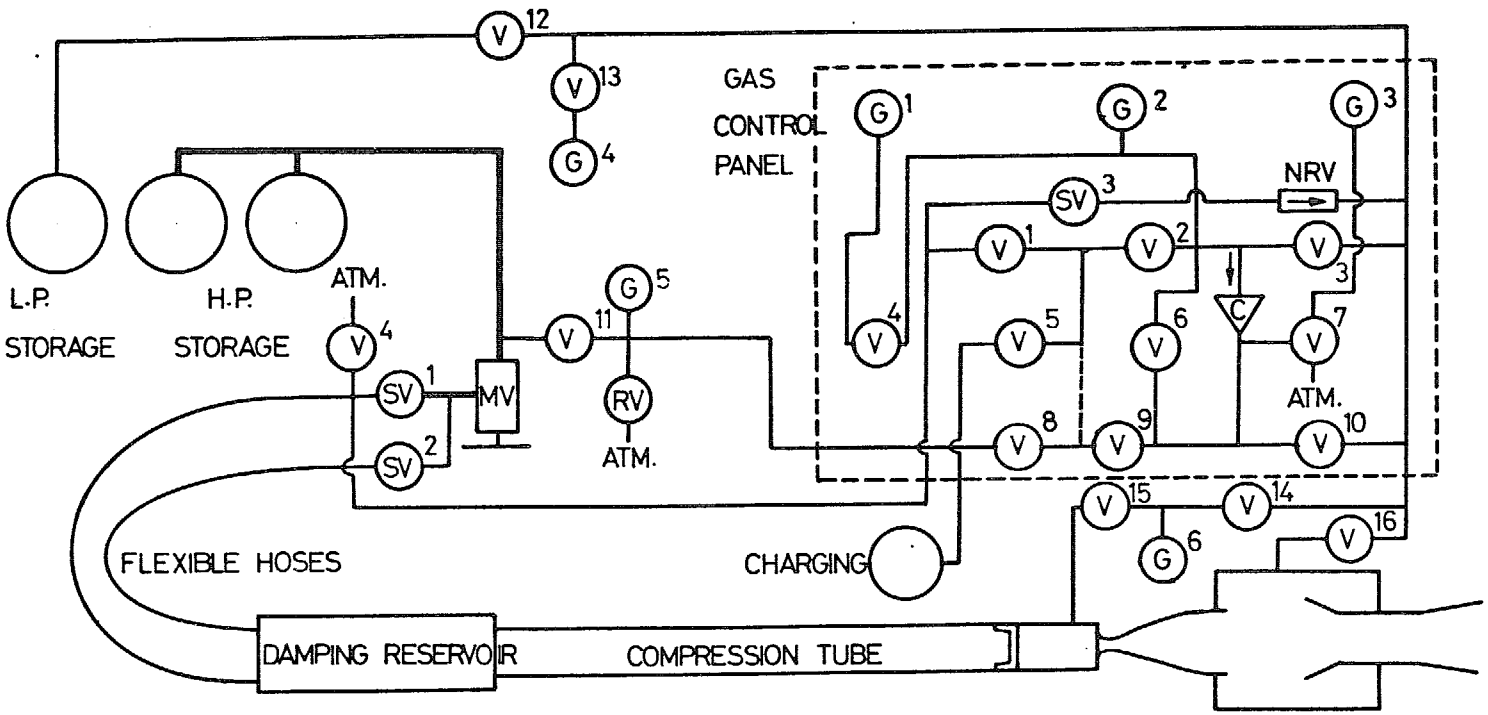

Fig 10 Sketch of tunnel gas-supply system

1 Stagnation pressure, 62 bar at 12 bar/div

2 Stagnation temperature, ref, 595°K at 50°C/div

3 Pitot pressure, 11 cm downstream of nozzle exit plane 5.2 cm above and below the jet-centre

Time scale 50 ms/div

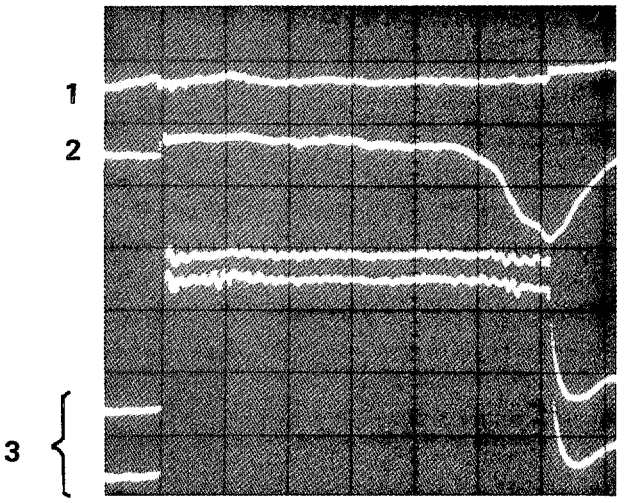

Fig 11 Records of flow pressures and temperature

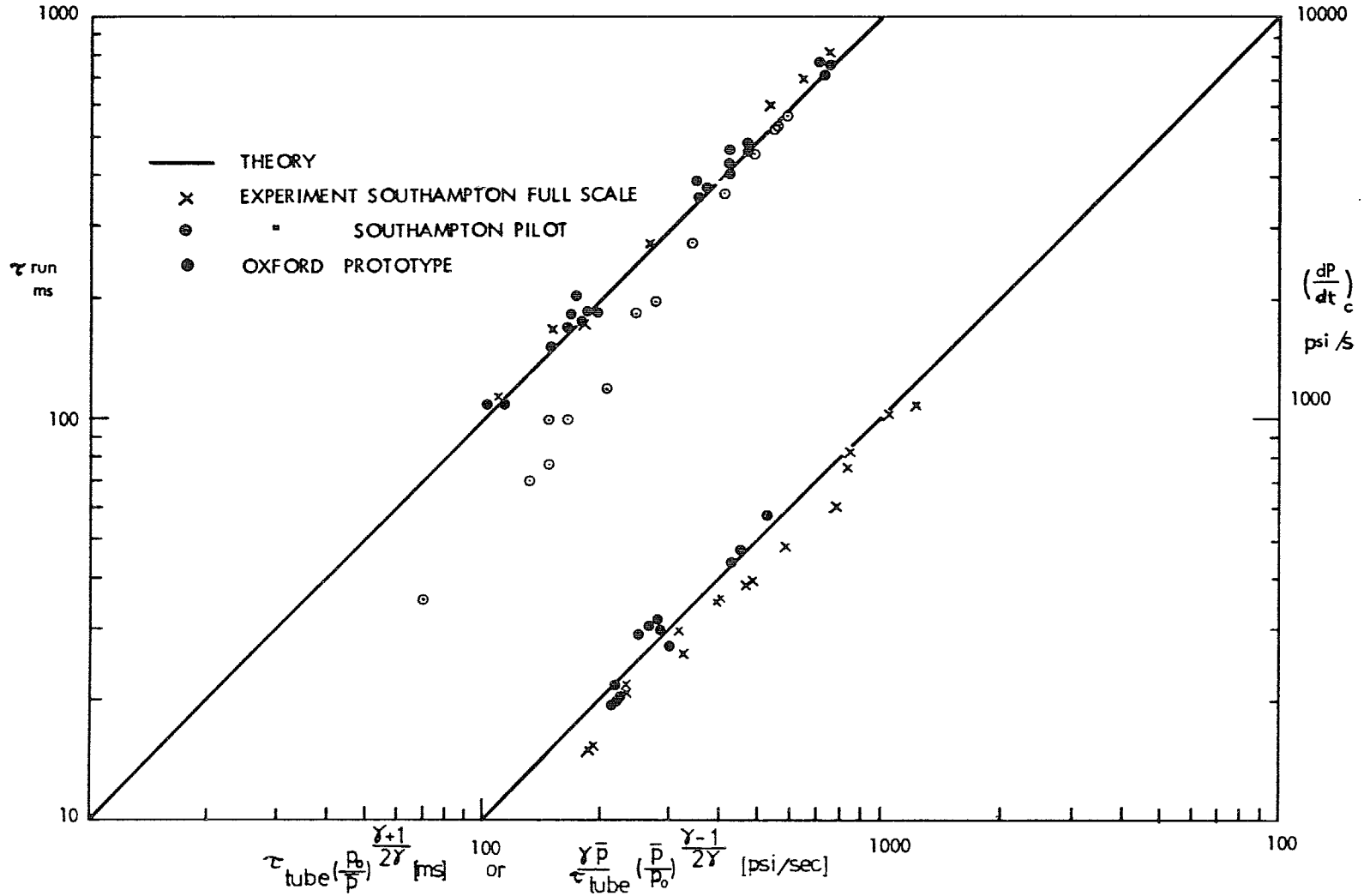

Fig 12 The running time and rate of rise of pressure during compression

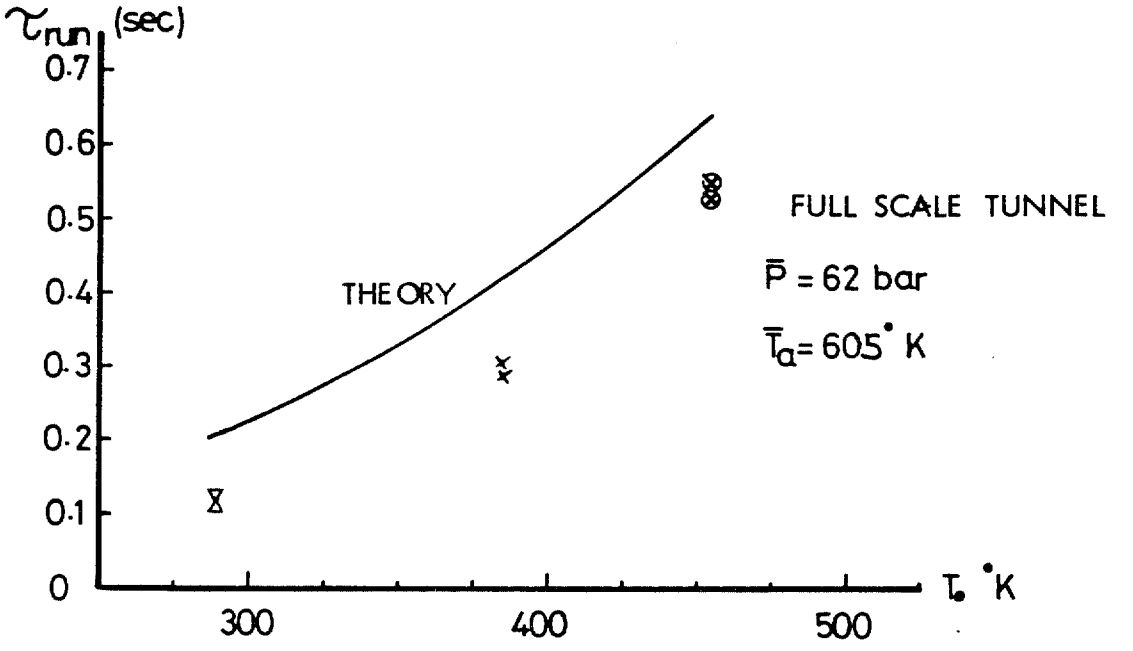

Fig 13 Running time vs initial temperature of test gas

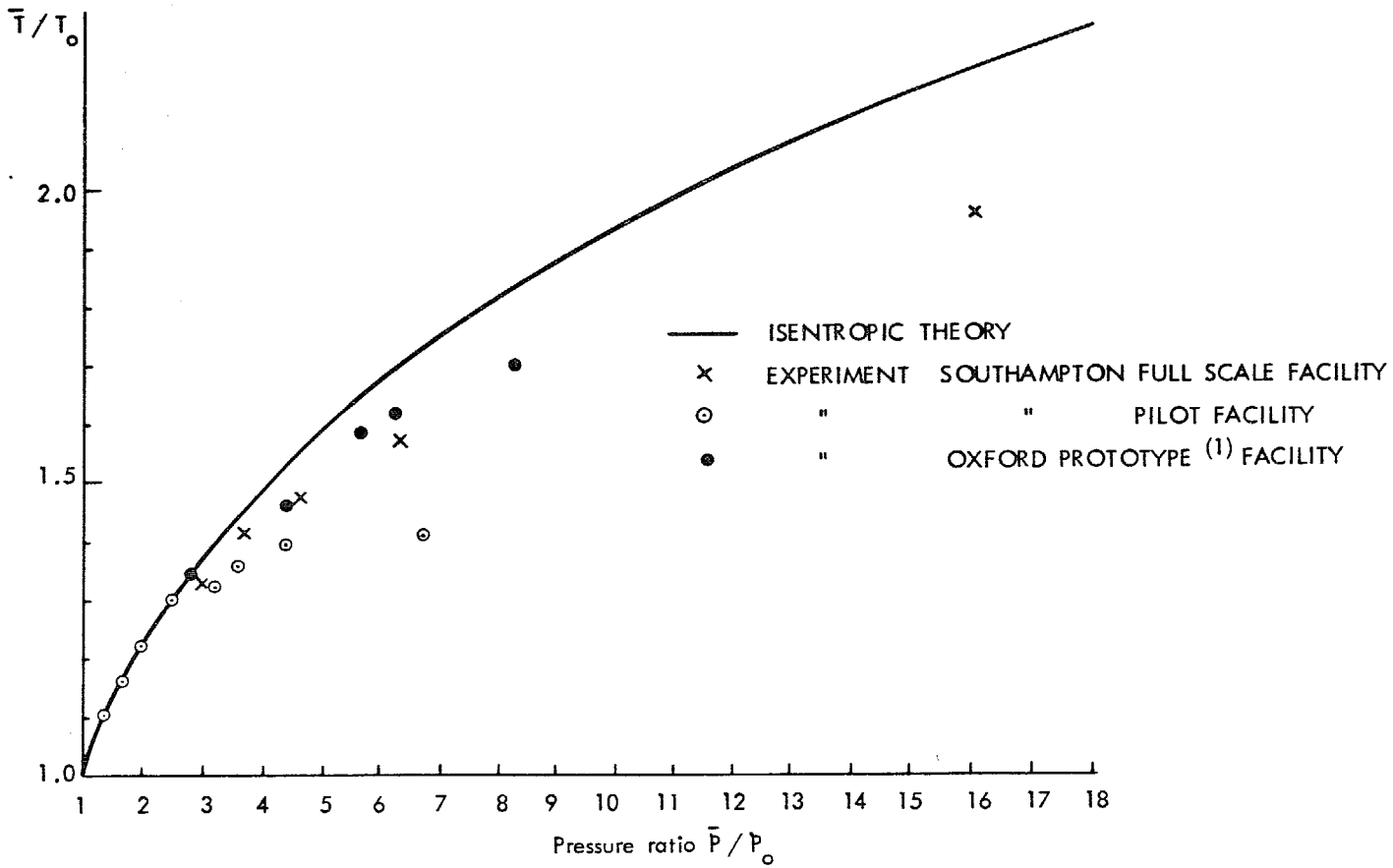

Fig 14 Peak flow temperature for various matching pressure ratios

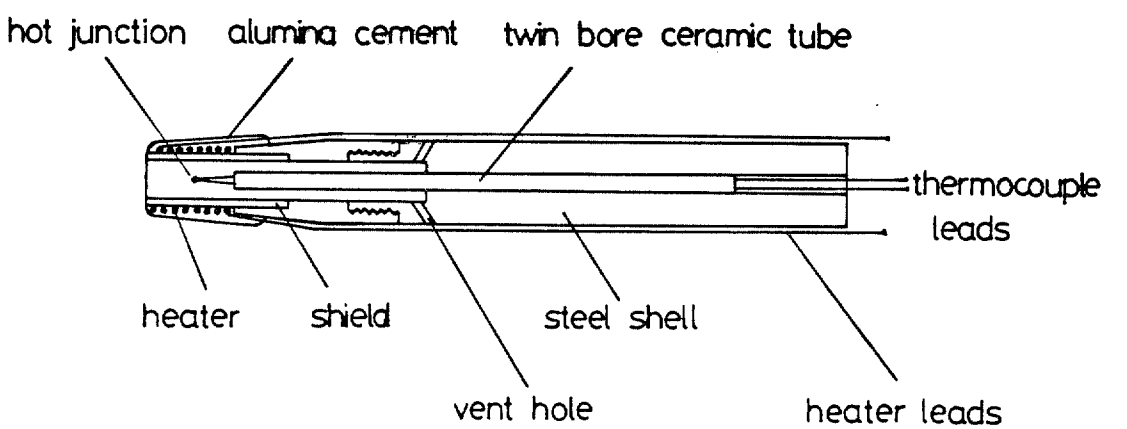

Fig 15 Thermocouple probe with a heated shield

Fig 16

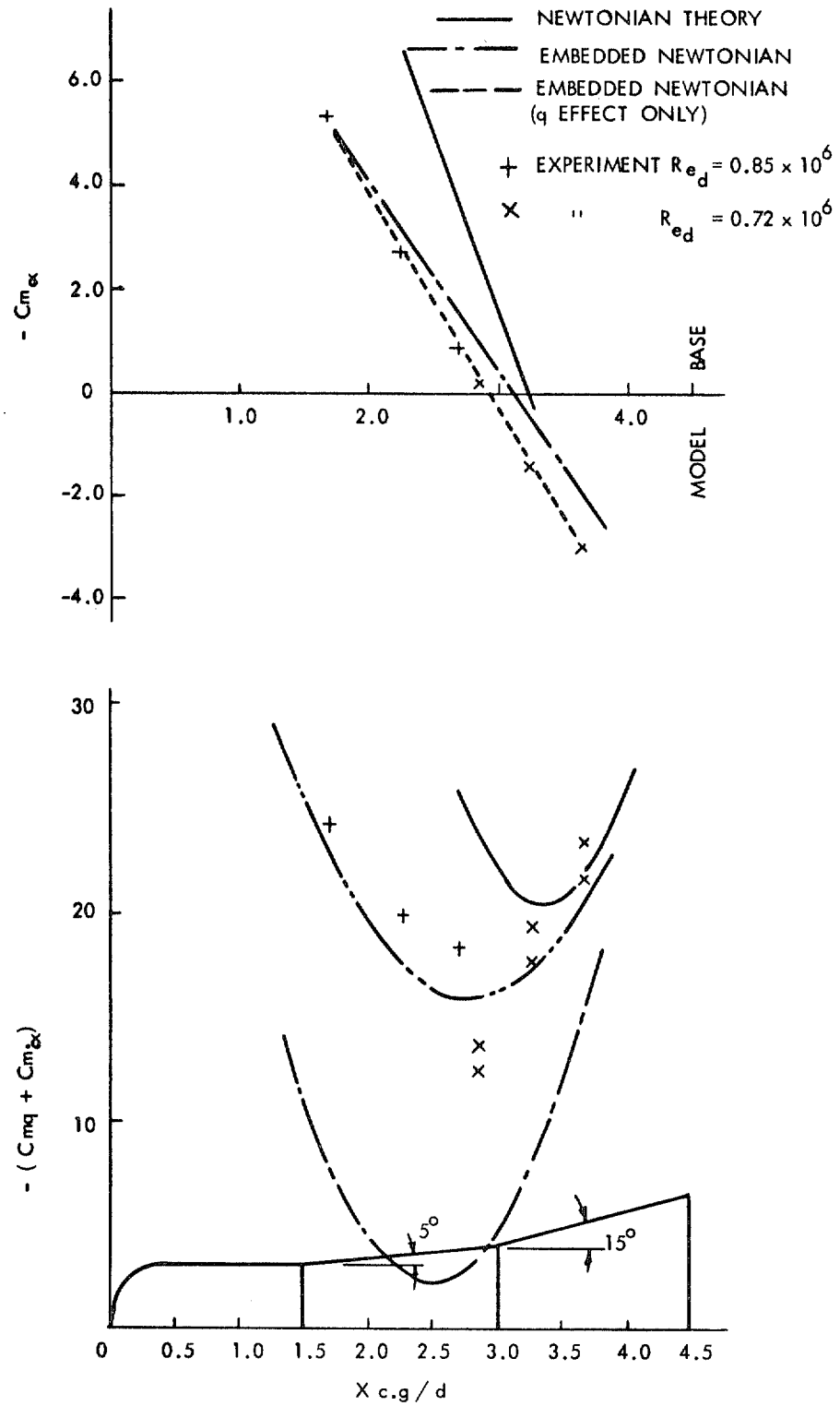

Fig 16 Stability derivatives of the model HBS at zero angle of attack

Printed in England for Her Majesty's Stationery Office by the Royal Aircraft Establishment, Farnborough. Dd.596060 K4 2/80.

First published 1980

HER MAJESTY'S STATIONERY OFFICE

Government Bookshops
49 High Holborn, London WC1V 6HB
13a Castle Street, Edinburgh EH2 3AR
41 The Hayes, Cardiff CF1 1JW
Brazennose Street, Manchester M60 8AS
Southey House, Wine Street, Bristol BS1 2BQ
258 Broad Street, Birmingham B1 2HE
80 Chichester Street, Belfast BT1 4JY

Government Publications are also available through booksellers

R & M No. 3844
ISBN 011471178*